J Nanopart Res (2011) 13:4929–4936
DOI 10.1007/s11051-011-0471-3

RESEARCH PAPER

Electrical characterization and Raman spectroscopy of individual vanadium pentoxide nanowire

W.-J. Shen · K. W. Sun · C. S. Lee

Received: 22 April 2011 / Accepted: 19 June 2011 / Published online: 6 July 2011
© Springer Science+Business Media B.V. 2011

Abstract We measured *I–V* characteristics, electrical resistance, and Raman spectra in the temperature range from room temperature to above 600 K to obtain nanodevices. Measurements were taken on a single V_2O_5 nanowire deposited on a Si template, where two- and four-point metallic contacts were previously made using e-beam lithography. In both two- and four-point probe measurements, the *I–V* curves were clearly linear and symmetrical with respect to both axes. Drastic reduction in electrical resistance and deviation from single valued activation energy with increasing temperature indicated phase transitions taking place in the nanowire. From temperature-dependent HR-Micro Raman measurements, reductions from V_2O_5 to VO_2/V_2O_3 phases took place at a temperature as low as 500 K, when electrons were injected to the nanowire through electrical contacts.

Keywords Dielectrophoresis · Metal oxide · Phase transition · Nanowire

W.-J. Shen · K. W. Sun (✉) · C. S. Lee
Department of Applied Chemistry, National Chiao Tung University, Hsinchu 30010, Taiwan
e-mail: kwsun@mail.nctu.edu.tw

Introduction

Recently, there has been a great interest on new types of nanodevices based on metal-oxide nanowires or nanotubes. Metal oxides with one-dimensional (1D) structures, such as a nanowire, nanotube, nanorods, and nanoribbon, show unique physical and chemical properties because of their large surface area and unique shape, making these materials effective for applications in photovoltaic devices (Nishio and Kakihana 2002; Law et al. 2005; Cheng et al. 2006), field emission display (Zhou et al. 2007; Chen et al. 2008), and so on. Therefore, synthesizing novel metal-oxide nanostructures and probing their intrinsic properties are critical to assess their possible role in new types of nanoscale devices.

Among these metal oxide semiconductors, vanadium pentoxide has attracted considerable interest over the years owing to its wide range of applications. Vanadium oxide and its derivated compounds (Zavalij and Whittingham 1999) have been applied in catalytic and electrochemical fields due to their outstanding structural flexibility combined with chemical and physical properties (Braithwaite et al. 1999; Spahr et al. 1999). Vanadium pentoxide oxide phase crystallized in 2D network structures can be regarded as a layered structure compound in which VO_5 square pyramids with a 5-fold coordination of vanadium and oxygen atoms are connected by sharing corners and edges (Bachmann et al. 1961). V_2O_5 has a bandgap of $\sim$2.5 eV. Prospective applications include photo- and electro-chromic devices (Nishio and Kakihana 2002; Cheng et al. 2006), chemical and gas sensing (Oyama et al. 1989; Raible et al. 2005; Mao et al. 2006; Dhayal Raj et al. 2010), catalysis (Chen et al. 2006), and positive electrodes of rechargeable lithium battery (Chan et al. 2007; Protasenko et al. 2007).

V_2O_5 with a 1D nanostructure has been successfully synthesized via template-assisted growth (Shi et al. 2007), surfactant/inorganic self-assembly, e-beam sputtering, chemical vapor deposition (Diaz-Guerra and Piqueras 2008), pulse laser deposition (Barreca et al. 2000; Ramana et al. 2005), hydrothermal approach (Shi et al. 2007; Chen et al. 2008; Mai et al. 2008; Zhou et al. 2008), and vapor pyrolytic deposition (Wu and Lee 2009). The electrical transport mechanism in V_2O_5 nanofibers has been studied in detail (Kim et al. 2000; Muster et al. 2000) at low temperature and room temperature. The conductivity of an individual V_2O_5 fiber was estimated to be $\sim$0.5 S/cm at 300 K. N-type enhancement FET-like behavior was demonstrated for individual V_2O_5 nanofibers at low temperature. The charge transport takes place through electron hopping between V^{IV} (impurities) and V^{V} centers. Chemiresistor-type gas sensors with high sensitivity and selectivity to amines were fabricated by depositing V_2O_5 nanofibers onto silicon templates (Raible et al. 2005). More recently, current–voltage (*I*–*V*) characteristics and electrical resistance were measured on V_2O_{5-x}–polyaniline nanorods with inter-digital metallic contacts made by lithography (Ferrer-Anglada et al. 2001) from 300 to 140 K. The *I*–*V* curves were nonlinear and symmetrical with electrical conductivity values near 0.1 S/cm at room temperature.

In this study, resistivity of a single V_2O_5 nanowire and contact resistance were accurately determined using three different probe schemes at room temperature. The wire was also transformed from a phase of pure V_2O_5 into mixed phases containing V_2O_3 and VO_2 at a temperature as low as 500 K when under electrical bias.

Experimental

Our V_2O_5 nanowires were grown on a conducting glass substrate combining gaseous transport and pyrolytic deposition of vanadium polyoxometalate anions, which yield vertically aligned V_2O_5 nanowires. The XRD pattern of the nanowires was indexed to the orthorhombic V_2O_5 structures. No signals due to impurity phases were detected. The HR-TEM image and SAED pattern confirm that the grown nanowires are single crystalline in nature and grown preferentially along one direction [010]. The synthesized V_2O_5 wires show ribbon-like morphology with an average width within 200–500 nm and a length up to several tens of micrometers. Details of the crystal growth and characterizations have been published elsewhere (Wu and Lee 2009).

Fabrication processes of the single nanowire-based devices are given as follows. The V2O5 nanowire powder was first diluted in 10 mL deionized (DI) water and ethanol (or acetone) mixture. The solution was then placed in an ultrasonic bath operated at a vibration frequency of 185 kHz for 30 min to prevent cluster formation. A test drop of the solution was placed on a bare Si wafer. After the solution dried out, scanning electron microscope (SEM) images were taken to examine nanowire clustering. The concentration of the solution was continuously diluted and adjusted until the nanostructures can be well dispersed on the Si template.

Two- and four-point metal contacts on Si templates were designed and fabricated to position a dispersed single nanowire. The templates used were commercially available 4-inch silicon wafers with (001) crystal orientation and n-type background doping. The surface of the Si substrate was passivated in advance using a thermally grown SiO_2 layer with a thickness of 2000 Å. This was to avoid leakage current through the substrate during *I*–*V* measurements. The Si wafer was first diced into 2 × 2 cm chips. A pattern of two-dimensional arrays of cross-finger-type Al or Ti/Au pads with a line width of $\sim$2 μm, a pitch from 2 to 10 μm, and a length of $\sim$15 μm were defined on the Si chip using e-beam lithography within an area of 1 mm^2.

Results and discussion

A drop of the properly diluted V2O5 nanowire solution was placed within the inter-digitated electrode patterns. By applying electrical bias across the contact pads, the dielectrophoresis force (Yamamoto

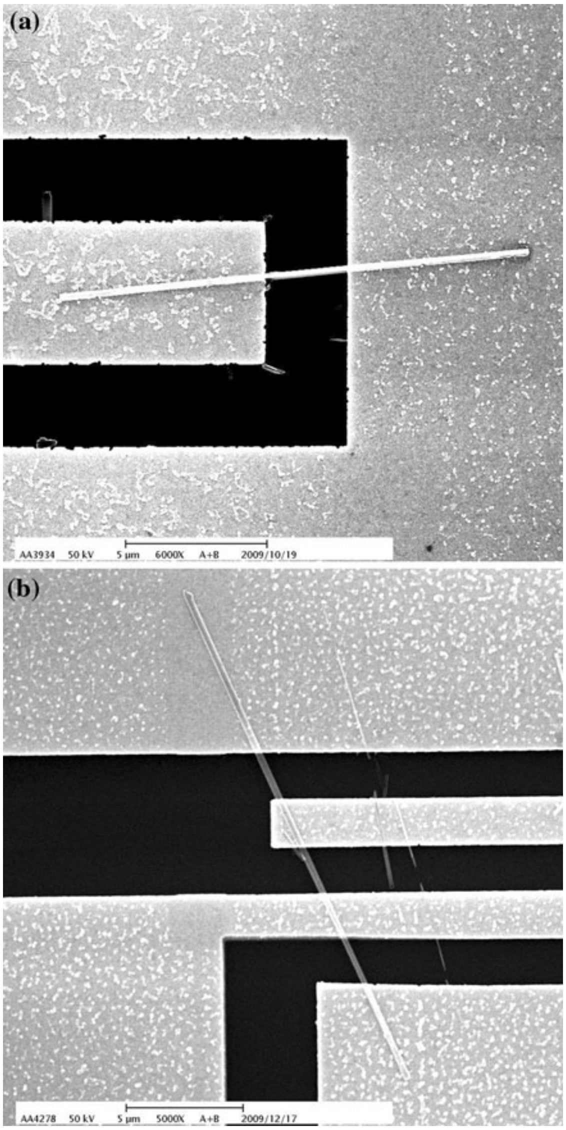

Fig. 1 **a** and **b** Nanowires aligned across the gaps between electrodes due to the dielectrophoresis force

et al. 1996; 1998; Choi et al. 2001; Suehiro et al. 2003) drove the nanowires to bridge the electrode gap. The SEM images of the V2O5 nanowires' dielectrophoresis alignment process across the interdigitated electrodes are shown in Fig. 1. The sample surface was scanned by SEM to allocate a single nanowire across two or four metal contacts. After a single nanowire was selected, a focus ion beam (FIB) was used to selectively deposit Platinum (Pt) metal contacts on the wires, as shown in Fig. 2. The patterned single nanowire was examined with EDX to ensure it was not contaminated during the FIB

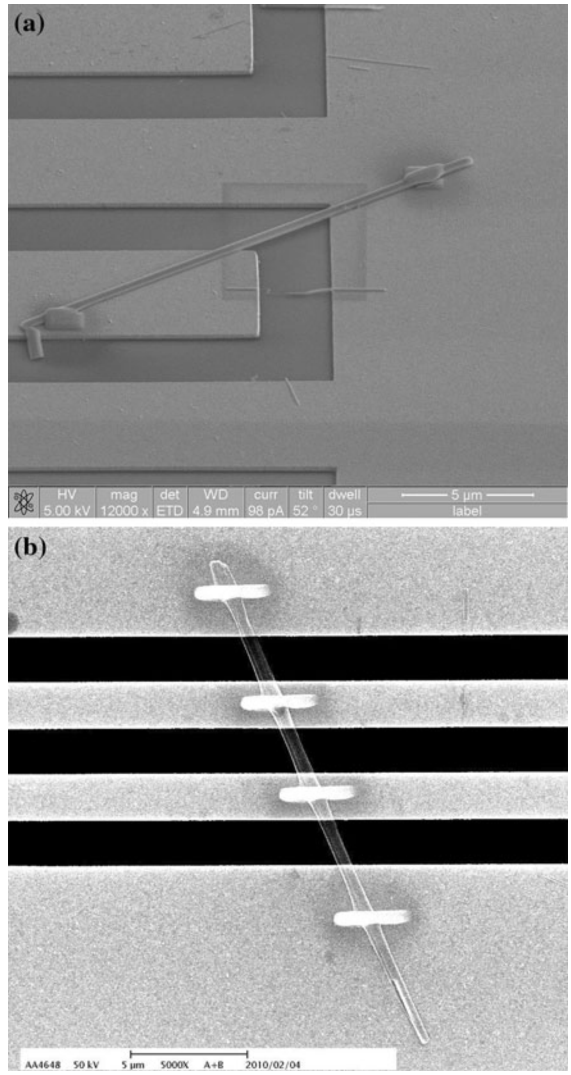

Fig. 2 **a** and **b** Contacts to electrodes were made by depositing Platinum (Pt) metal on the nanowires using focusing ion beam

process. Temperature dependence of the *I*–*V* characteristics of a single V_2O_5 nanowire was probed at a temperature range from 300 to 640 K. This was done with an HP-4145 probe station under current sensitivity of 1 pA and heating stage. The resistivity of the single nanowire at 300 K was determined with three different probe schemes: (a) Two-point contact probe (sweep voltage mode), where current through the wire was measured by sweeping the voltage from −0.5 to 0.5 V with a step of 0.001 V; (b) Four-point contact probe (sweep current mode), where current was supplied through outer electrodes and voltage drop was determined between two inner electrodes;

and (c) Four-point contact probe, where resistivity of the nanowire was determined using an algorithm developed (Gu et al. 2006). The Raman spectra of the single wire under the temperature-dependent electrical measurements were monitored at the same time through a confocal microscope. The spectra were then analyzed by a 0.8 m spectrometer equipped with liquid nitrogen cooled CCD detector at the excitation wavelength of 633 nm.

Figure 3 shows the *I–V* curve of a nanowire dispersed in ethanol and prepared on two-point Al electrodes. At room temperature, the sample exhibited slightly nonlinear, symmetrical *I–V* characteristics. The Schottky type contact resistance between the nanowire and Al contact was due to the nanowire adsorption of ethanol molecules (Liu et al. 2005). The contact problem was solved when nanowires were dispersed in solutions containing no hydrogen bonds, such as acetone. Figure 4 shows the improved *I–V* characteristics of the single wire dispersed in acetone and prepared on two-point Au electrodes. Contact between the wire and the electrodes now show linear and symmetrical behavior. A resistivity of 6.61 Ω cm of the device was derived from various samples. Contact resistance can be determined by comparing results between two- and four-point probe measurements. The single wire resistivity determined with probe scheme (b) is 5.87 Ω cm, resulting in a contact resistance ~50.305 KΩ. The resistivity value was further verified using probe scheme (c). The schematic of probe scheme (c) and the parameters used to derive the resistivity are summarized in Table 1. The derived resistivity is 5.65 Ω cm, which is very close to the result determined from probe scheme (b).

Following the electrical characterization of the single wire at room temperature, individual nanowires were placed on a heating stage in a chamber. Measurements of temperature dependence in conductivity were first carried out at atmosphere in the temperature range 300–580 K. The resistance of the single nanowire is plotted in Fig. 5 as ln(*T*/*R*) versus reciprocal temperature. Electrical conduction in V_2O_5 is generally believed to proceed by hopping between V^{5+} and V^{4+} impurity centers (Livage 1991; Muster et al. 2000). An increase in conductivity with increasing temperature was revealed, consistent with thermally activated hopping transport. However, the curve departed significantly from linearity when the

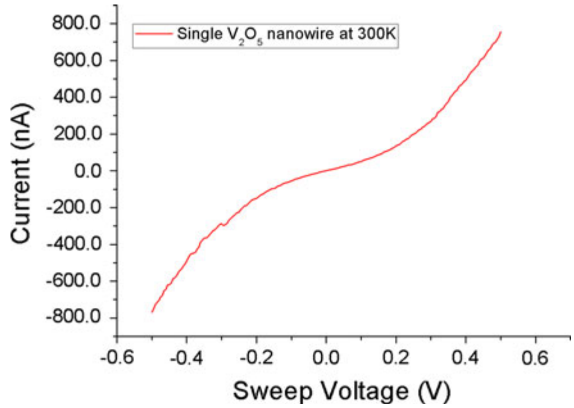

Fig. 3 *I–V* characteristics of the single nanowire dispersed in ethanol at room temperature

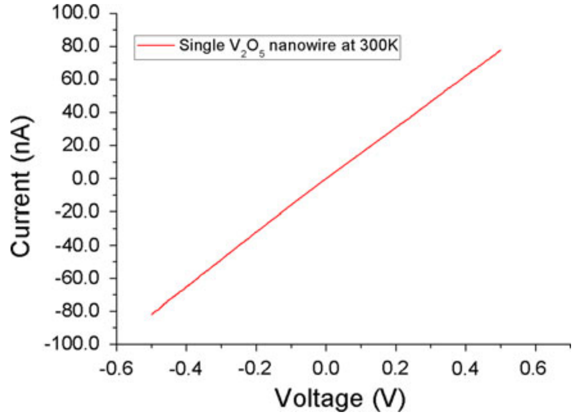

Fig. 4 *I–V* characteristics of the single nanowire dispersed in acetone at room temperature

plot of ln(*T*/*R*) versus 1/*T* in Fig. 5 was analyzed using a model proposed by Mott (1968) for small polaron hopping in transition metal oxides. A similar behavior was also observed in electrical measurements at lower temperature (Muster et al. 2000). This has been attributed to the temperature dependence of the hopping activation energy, which includes a disorder energy associated to the random material structure (Bullot et al. 1980). The departure from linearity was even more pronounced when the temperature was further increased. We also noted that the conductivity of the nanowire was not completely restored to its original value after it cooled down to room temperature. On the other hand, the nanowire was relatively stable if simply heated it up to 600 K without applying electrical bias. Therefore, a phase transformation is suspected to be taking

Table 1 Schematic of the probe scheme (c) and parameters used to derive the resistivity of the single wire

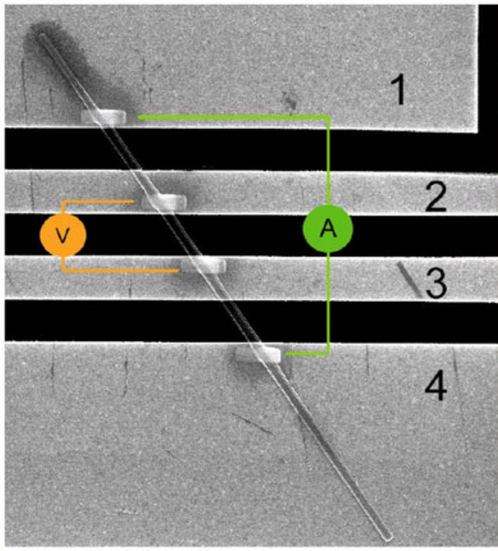

$R^*_{13} = 2{,}095{,}487\ \Omega$	$R_{14} = 960{,}900\ \Omega$
$R_{23} = 818{,}186\ \Omega$	$R_{24} = 446{,}812\ \Omega$
$L^*_{24} = 2.059\ \mu m = 2.059\times10^{-4}$ cm	
$\Delta R = (R_{13}-R_{14}) + (R_{24}-R_{23}) = (R_{L13}-R_{L14}) + (R_{L24}-R_{RL23})$	
$\Delta L = (L_{13}-L_{14}) + (L_{24}-L_{23}) = 2L_{24}$	
S (cross-section area of the wire) $S = \pi D^2 / 4 = 3.05\times10^{-9}$ cm^2 D = 623 nm (diameter)	
*R_{ab} & L_{ab}: resistance and length between point a and point b	
$\rho = S\,(\Delta R/\Delta L) = S\,[(R_{L13}-R_{L14})+(R_{L24}-R_{L23})] / 2_{L24}$	

place during heating processes, and the phase transitions are facilitated by the injection of electrons through the contacts.

In the next experiments, the sample chamber was pumped down and flushed with dry N_2 three times. Then, the temperature-dependent measurements in conductivity were carried out both in vacuum and at

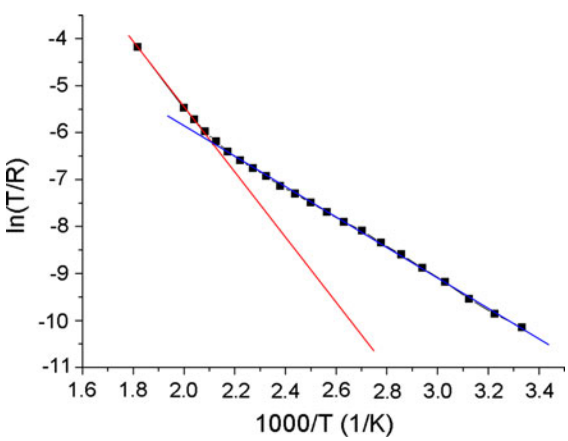

Fig. 5 Temperature dependence of the single nanowire measured at atmosphere. The plot was approximated by a straight line (in *red color*) in the high temperature range ($T > 500$ K). (Color figure online)

an inert gas (N_2) filled environment at the temperature range of 300–550 K. Figure 6 shows the resistance of the single nanowire plotted as ln(T/R) versus reciprocal temperature. The resistance of the nanowire dropped by three orders of magnitude from 1.7 MΩ at 300 K to 1.725 KΩ at 550 K. The latter value was maintained without breaking the vacuum after the wire cooled down to 300 K. The curve in Fig. 6 strongly deviated from a linear plot. During the measurements, evolutions of the Raman spectra as a function of temperature were also monitored simultaneously at each temperature increment step. The Raman spectrum of the V_2O_5 nanowire recorded before the temperature-dependent electrical measurements is shown in Fig. 7a. The Raman lines at 143, 283, 404, 482, 525, 699, and 994 cm^{-1} are assigned to V_2O_5 in its orthorhombic phase (Oyama et al. 1989; Wang and Gonsalves 1999). As the temperature was increased to above 500 K, changes were observed in the spectra and new lines began to appear. The Raman spectrum of the sample at the end of the temperature cycle is given in Fig. 7b. The assignment of the peaks is summarized in Table 2. After comparing our results with Raman spectra from pure V_2O_3 and VO_2, we conclude that the reduction

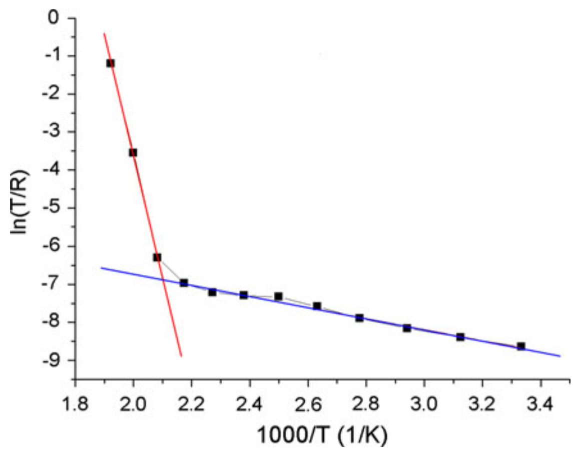

Fig. 6 Temperature dependence of the single nanowire measured in vacuum. The plot is approximated by a straight line (in *red color*) in the high temperature range ($T > 480$ K). (Color figure online)

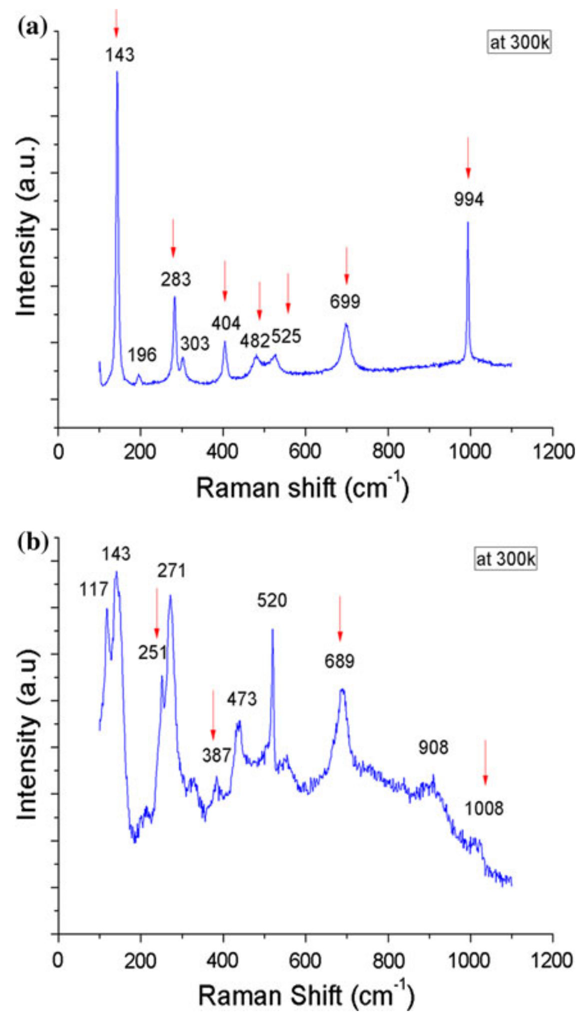

Fig. 7 Raman spectrum of the single V_2O_5 nanowire under electrical bias **a** at the beginning of temperature cycle and **b** at the end of the temperature cycle. Peaks in **a** indicated by *red arrows* are signatures from the V_2O_5 phase. Peaks in **b** indicated by *red arrows* are signatures from the VO_2/V_2O_3 phase. (Color figure online)

in resistance of nanowire is most likely due to the appearance of the V_2O_3 and VO_2 phases. Self-assembled VO_2 nanowires have been synthesized by pyrolysis of $(NH_4)_{0.5}V_2O_5$ nanowires in vacuum at a temperature as high as 800–870 K (Wu et al. 2005). However, transitions into V_2O_3 and VO_2 phases can take place at a temperature as low as 500 K when the V_2O_5 nanowire is under electrical bias, i.e., electrons are supplied through the contact to the nanowire. The change in resistance was clearly more drastic when temperature-dependent measurements were carried out in the inert gas filled environment and in vacuum. This is because that transitions to V_2O_3 and VO_2 phases are hampered by the re-oxidation process when the nanowire is exposed to the O_2. This is also the reason why the resistance of the nanowire maintains at its final value in inert gas filled and vacuum environment.

Summary

In conclusion, the transport properties and temperature dependence in conductivity of single V_2O_5 nanowires using e-beam lithography, FIB, and di-electrophoresis techniques were reported. *I–V* characteristics showed linear and symmetric behavior through the entire temperature range, which indicated that the contacts are ohmic. The resistivity and contact resistance were accurately determined using three different probe schemes. Resistance of the single V_2O_5 nanowire decreased with increasing temperature due to the occurrence of mixed V_2O_3/VO_2 phases. The temperature dependence of the nanowire transport characteristics shows a drastic reduction in electrical resistivity (by three orders of magnitude) at a temperature near 550 K. Evidence from the Raman spectra indicate that phase transitions take place at a temperature as low as 500 K when the nanowire is under an electrical bias.

Table 2 List of peak assignment of the Raman spectrum shown in Fig. 7b

Raman peak (cm^{-1})	Assignment
117	Acetone
143	V_2O_5 (V–O–V sym-related stretch)
251	V_2O_3
271	Gold electrode (Au)
387	VO_2 (Ag mode)
437	Ethanol (C–C–O in-plane bend)
520	Si substrate (Si)
689	$V_2O_3^{4+}$ (V–O–V)
908	ACE (C–C stretch)
1008	$V_2O_3 + (V = 0)$

Acknowledgment This study was supported by a grant from the National Science Council, ROC (NSC 99-2119-M-009-004-MY3).

References

Bachmann HG, Ahmed FR, Bames WH (1961) The crystal structure of vanadium pentoxide. Z Kristallogr 115:110–131

Barreca D, Armelao L, Caccavale F, Di Noto V, Gregori A, Rizzi GA, Tondello E (2000) Highly oriented V2O5 nanocrystalline thin films by plasma-enhanced chemical vapor deposition. Chem Mater 12:98–103

Braithwaite JS, Catlow CRA, Gale JD, Harding JH (1999) Lithium intercalation into vanadium pentoxide: a theoretical study. Chem Mater 11:1990–1998

Bullot J, Gallais O, Gauthier M, Livage J (1980) Semiconducting properties of amorphous V2O5 layers deposited from gels. Appl Phys Lett 36:986–988

Chan CK, Peng HL, Twesten RD, Jarausch K, Zhang XF, Cui Y (2007) Fast, completely reversible Li insertion in vanadium pentoxide nanoribbons. Nano Lett 7:490–495

Chen LY, Yang BL, Zhang XC, Dong W, Cao K, Zhang XP (2006) Methane oxidation over a V2O5 catalyst in the liquid phase. Energy Fuels 20:915–918

Chen W, Zhou CW, Mai LQ, Liu YL, Qi YY, Dai Y (2008) Field emission from V2O5 center dot *n*H(2)O nanorod arrays. J Phys Chem C 112:2262–2265

Cheng K, Chen F, Kai J (2006) V2O5 nanowires as a functional material for electrochromic device☆. Sol Energy Mater Sol Cells 90:1156–1165

Choi WB, Jin YW, Kim HY, Lee SJ, Yun MJ, Kang JH, Choi YS, Park NS, Lee NS, Kim JM (2001) Electrophoresis deposition of carbon nanotubes for triode-type field emission display. Appl Phys Lett 78:1547

Dhayal Raj A, Pazhanivel T, Suresh Kumar P, Mangalaraj D, Nataraj D, Ponpandian N (2010) Self assembled V2O5 nanorods for gas sensors. Curr Appl Phys 10:531–537

Diaz-Guerra C, Piqueras J (2008) Thermal deposition growth and luminescence properties of single-crystalline V2O5 elongated nanostructures. Cryst Growth Des 8:1031–1034

Ferrer-Anglada N, Gorri JA, Muster J, Liu K, Burghard M, Roth S (2001) Electrical transport and AFM microscopy on V2O5-x-polyaniline nanorods. Mater Sci Eng C 15:237–239

Gu Wenhua, Choi Hyungsoo, Kim Kyekyoon (2006) Universal approach to accurate resistivity measurement for a single nanowire: theory and application. Appl Phys Lett 89:253102

Kim GT, Muster J, Krstic V, Park JG, Park YW, Roth S, Burghard M (2000) Field-effect transistor made of individual V2O5 nanofibers. Appl Phys Lett 76:1875–1877

Law M, Greene LE, Johnson JC, Saykally R, Yang PD (2005) Nanowire dye-sensitized solar cells. Nat Mater 4:455–459

Liu JF, Wang X, Peng Q, Li YD (2005) Vanadium pentoxide nanobelts: highly selective and stable ethanol sensor materials. Adv Mater 17:764–767

Livage J (1991) Vanadium pentoxide gels. Chem Mater 3:578–593

Mai LQ, Guo WL, Hu B, Jin W, Chen W (2008) Fabrication and properties of VO*x*-based nanorods. J Phys Chem C 112:423–429

Mao CJ, Pan HC, Wu XC, Zhu JJ, Chen HY (2006) Sonochemical route for self-assembled V2O5 bundles with spindle-like morphology and their novel application in serum albumin sensing. J Phys Chem B 110:14709–14713

Mott NF (1968) Conduction in glasses containing transition metal ions. J Non-Cryst Solids 1:1–17

Muster J, Kim GT, Krstic V, Park JG, Park YW, Roth S, Burghard M (2000) Electrical transport through individual vanadium pentoxide nanowires. Adv Mater 12:420–424

Nishio S, Kakihana M (2002) Evidence for visible light photochromism of V2O5. Chem Mater 14:3730–3733

Oyama ST, Went GT, Lewis KB, Bell AT, Somorjai GA (1989) Oxygen chemisorption and laser Raman spectroscopy of unsupported and silica supported vanadium oxide catalysts. J Phys Chem 93:6786–6790

Protasenko V, Gordeyev S, Kuno M (2007) Spatial and intensity modulation of nanowire emission induced by mobile charges. J Am Chem Soc 129:13160–13171

Raible I, Burghard M, Schlecht U, Yasuda A, Vossmeyer T (2005) V2O5 nanofibres: novel gas sensors with extremely high sensitivity and selectivity to amines. Sensors Actuators B Chem 106:730–735

Ramana CV, Smith RJ, Hussain OM, Chusuei CC, Julien CM (2005) Correlation between growth conditions, microstructure, and optical properties in pulsed-laser-deposited V2O5 thin films. Chem Mater 17:1213–1219

Shi SF, Cao MH, Fle XY, Xie HM (2007) Surfactant-assisted hydrothermal growth of single-crystalline ultrahigh-aspect-ratio vanadium oxide nanobelts. Cryst Growth Des 7:1893–1897

Spahr ME, Stoschitzki-Bitterli P, Nesper R, Haas O, Novak P (1999) Vanadium oxide nanotubes—a new nanostructured redox-active material for the electrochemical insertion of lithium. J Electrochem Soc 146:2780–2783

Suehiro J, Zhou GB, Hara M (2003) Fabrication of a carbon nanotube-based gas sensor using dielectrophoresis and its application for ammonia detection by impedance spectroscopy. J Phys D Appl Phys 36:L109–L114

Wang JZ, Gonsalves KE (1999) A combinatorial approach for the synthesis and characterization of polymer/vanadium oxide nanocomposites. J Comb Chem 1:216–222

Wu MC, Lee CS (2009) Field emission of vertically aligned V2O5 nanowires on an ITO surface prepared with gaseous transport. J Solid State Chem 182:2285–2289

Wu X, Tao Y, Dong L, Wang Z, Hu Z (2005) Preparation of VO2 nanowires and their electric characterization. Mater Res Bull 40:315–321

Yamamoto K, Akita S, Nakayama Y (1996) Orientation of carbon nanotubes using electrophoresis. Jpn J Appl Phys 2 Lett 35:L917–L918

Yamamoto K, Akita S, Nakayama Y (1998) Orientation and purification of carbon nanotubes using ac electrophoresis. J Phys D Appl Phys 31:L34–L36

Zavalij PY, Whittingham MS (1999) Structural chemistry of vanadium oxides with open frameworks. Acta Crystallogr B Struct Sci 55:627–663

Zhou CW, Mai LQ, Liu YL, Qi YY, Dai Y, Chen W (2007) Synthesis and field emission property of V2O5 center dot nH(2)O nanotube arrays. J Phys Chem C 111:8202–8205

Zhou F, Zhao XM, Yuan CG, Li L (2008) Vanadium pentoxide nanowires: hydrothermal synthesis, formation mechanism, and phase control parameters. Cryst Growth Des 8:723–727